

Probing tumor microtissue formation and epithelial-mesenchymal transition on a well-mesh microchip

Cite as: Biomicrofluidics 13, 014102 (2019); doi: 10.1063/1.5064838

Submitted: 9 October 2018 · Accepted: 21 December 2018 ·

Published Online: 4 January 2019



View Online



Export Citation



CrossMark

Kaiyan Li, Xingyuan Yang, and Xinghua Gao^{a)}

AFFILIATIONS

Materials Genome Institute, Shanghai University, Shanghai 200444, China

^{a)}Author to whom correspondence should be addressed: gaoxinghua@t.shu.edu.cn. Tel.: +86-69982223.

ABSTRACT

Three-dimensional cultures of tumor microtissues and biomimetic simulation of tumor microenvironments are of great significance in the study of tumorigenesis and development processes. In this study, a well-mesh microchip was developed to realize the formation and culture of tumor microtissues *in vitro*. Human lung adenocarcinoma HCC827 cells and large-cell lung cancer NCI-H460 cells were used. The size and morphology of the microtissues have been observed. In addition, we constructed an *in situ* three-dimensional co-culture model with tumor cell microtissues (HCC827 or NCI-H460 cells), extracellular matrix (Matrigel), and human umbilical vein endothelial cells. HCC827 microtissue epithelial-mesenchymal transition (EMT) in the established well-mesh microchip also was investigated, and the results showed that recombinant transforming growth factor could activate the Snail and Akt gene and promote migration and EMT with the decrease of E-cadherin expression for HCC827. This well-mesh microchip features simple operation and easy observation, and could provide a new method for the study of tumor cells and tumor microenvironments *in vitro*. Therefore, this model has potential application value in organ-on-chip technology, tissue engineering, and drug evaluation.

Published under license by AIP Publishing. <https://doi.org/10.1063/1.5064838>

I. INTRODUCTION

In vitro cell culture is an indispensable and important aspect of cell biology, biochemistry, drug discovery and development, pharmacokinetic studies, and tissue engineering.¹ Presently, available *in vitro* cell culture models can be divided into two-dimensional culture models and three-dimensional culture models, of which the more traditional and easily realized is two-dimensional cell culture, such as well plate, culture flask, and dish. This culture model has played a significant role in biomedical research.^{2,3} However, it has considerable limitations. The model is unable to accurately represent complicated living tissue structures and functions, and cannot rebuild the complicated and dynamic microenvironment of the body. In comparison, *in vitro* three-dimensional cell culture models have advantages.^{4,5}

Three-dimensional cell culture models can better simulate the microstructures, dynamic mechanical properties, and

biochemical functions of the whole organs.^{6,7} They can facilitate the realization of control of cell differentiation and simulation of microstructures, which are impossible in conventional two-dimensional cell culture models.⁸ Presently, three-dimensional *in vitro* culture models can be simply classified according to whether or not they include cell scaffold materials. In models with scaffold material, the scaffold material is made of a biocompatible polymer or natural biological extract, such as poly (lactic-co-glycolic acid) (PLGA)⁹ or Matrigel,¹⁰ to provide a specific three-dimensional growth environment for cells. In three-dimensional cell culture models without scaffold material, multicellular spheroids¹¹ or microtissues¹² are formed by specific methods, including the hanging drop method and microwell array models formed on the basis of microfabrication and microfluidics. The specific method depends mainly on the characteristics of the cell itself. These models are not as widely applied as models that include scaffold material, but they eliminate the possible

effects of biological material on cells and have huge advantages for three-dimensional *in vitro* cell culture of specific systems such as tumor cells.^{11,13} Three-dimensional cell culture is of great significance in tumor formation and development and other aspects of cell culture, and it has been widely applied in multiple frontier fields such as biomimetics,¹⁴ tissue engineering,¹⁵ drug evaluation,^{16,17} and organ-on-chip techniques.^{18,19}

It is well known that tumor microenvironments are complicated systems composed of different types of cells and extracellular matrixes, and they play a significant role in tumor formation and development.^{20,21} The three-dimensional *in vitro* cell culture of tumor cells can be used to simulate a tumor microenvironment.^{22–26} The tumor cells can be cultured in spheroids, and thus three-dimensional *in vitro* cell culture of non-scaffold material can be performed to obtain tumor cell spheroids or tumor microtissues.²⁷ However, if the formed tumor cell spheroids or tumor microtissues are to be further used for simulating a tumor microenvironment, they need to be moved and fixed and may be destroyed in the process, resulting in many limitations in their actual application. Considering the importance and limitations of this method, we aimed to develop a simple three-dimensional *in vitro* cell culture model to achieve the formation and culture of tumor microtissues and further simulate tumor microenvironments *in vitro* by constructing a multi-factor system with an extracellular matrix, co-cultured cells, chemical stimuli, etc. In addition, during the tumor formation and development, tumor cells have epithelial-mesenchymal transition (EMT) and mesenchymal-epithelial transition (MET) processes repeatedly, and these processes include abnormal activation of multiple transcription factors, change of cell surface protein expression, and reorganization of cytoskeletal proteins, which are important processes for tumor invasion, spreading, and metastasis.^{28,29} Therefore, in addition to the formation and culture of tumor microtissues, we also study the tumor micro-tissue EMT process for a research purpose.

In view of the above aim, a three-dimensional cell culture model based on a well-mesh microchip was developed for the formation, culture, and observation of microtissue of human non-small-cell lung cancer (adenocarcinoma cell HCC827 and large-cell lung cancer cell NCI-H460). This model was further developed to encapsulate the extracellular matrix of tumor tissues, realize three-dimensional co-culture with human umbilical vein endothelial cells (HUVECs), and simulate the three-dimensional multi-factor tumor microenvironment by applying recombinant transforming growth factor (TGF- β) to study the expression of EMT-related protein and gene of HCC827 under different conditions and to investigate cell migration in a bionic three-dimensional microenvironment.

II. MATERIALS AND METHODS

A. Microwell array design and fabrication

Soft lithography etching technology was used to prepare the microwell array. First, a silicon slice was evenly coated with a layer of SU-8 3035 photoresist (Microchem), with a

thickness of about 250–300 μm . After soft baking, UV exposure, post exposure baking, developing, and other processes, an SU8 template for the microwell array was obtained. The template was processed with oxygen plasma, and then silanized by 1H,1H,2H,2H-perfluorooctyltriethoxysilane (POTS, Sigma). Finally, an appropriate amount of evenly mixed and defoamed polydimethylsiloxane (PDMS, Sylgard 184, Dow Corning) prepolymer solution (monomer:curing agent = 10:1) was put into the template, and another silanized PDMS slice with a flat surface was placed on the PDMS prepolymer solution and a weighted object was put on top to extrude the PDMS prepolymer solution, making the PDMS slice contact the SU8 template. After curing in an oven at 80 °C for 60 min, the membrane was peeled off the PDMS microwell array to obtain wafers with a diameter of 19 mm. In the microwell array, the microwell diameter was 1.5 mm, the distance between adjacent microwells was 1.5 mm, and the membrane thickness (measured with a Step Profiler) was approximately 260 μm .

B. Well-mesh microchip design and fabrication

In the experiment, the well-mesh microchip was mainly composed of four parts. The first part is confocal dish (NEST) with middle hole coated by PDMS. The second part is PDMS microwell array membrane with a diameter of 19 mm. The third part Nylon mesh with a diameter of 20 mm is a cell strainer (FALCON) with a pore diameter of 100 μm , as shown in the enlarged partial view in Fig. 1. The fourth part PDMS cell culture medium storage layer is a circle with an outer diameter of 22 mm and an inner diameter of 12 mm. The middle hole confocal dish modified by PDMS is sealed with a PDMS microwell array membrane with the oxygen plasma, and other parts are pasted with PDMS prepolymer solution as glue and then heated to form an integral. After that, the fabricated well-mesh microchip was processed with plasma, sterilized with ultraviolet for 30 min, soaked in 2% Pluronic F-127 (Sigma) for 1 h, and then rinsed with phosphate buffered solution (PBS) three times. After the addition of sterile culture medium, cells could be inoculated and cultured for subsequent experiments.

C. Cell culture and trans-differentiation

Human non-small-cell lung cancer adenocarcinoma HCC827 cells, large-cell lung cancer NCI-H460 cells, and HUVECs were used. HCC827 and NCI-H460 cells were purchased from the cell bank/stem cell bank of the Chinese Academy of Sciences (ATCC source) and culture medium from Roswell Park Memorial Institute Medium 1640 (1640, Gibco) containing 10% fetal bovine serum (FBS, Gibco) and 1% penicillin-streptomycin double antibody (Gibco). HUVECs were purchased from BeNa Chuanglian Biotechnology Co., Ltd. (ATCC source); the culture medium was Dulbecco's modified Eagle's medium with 4500 mg/l glucose (HG-DMEM, Gibco) containing 10% FBS and 1% penicillin-streptomycin double antibody. In addition, to study the tumor cell epithelial-mesenchymal transition (EMT), we used a 3% FBS

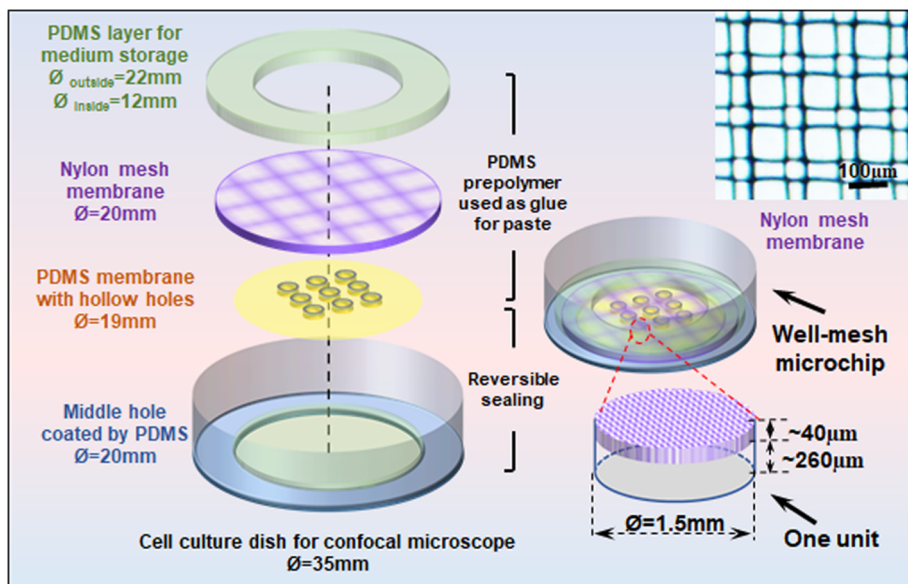


FIG. 1. The well-mesh microchip design and the image of the mesh membrane.

culture medium with transforming growth factor- β 1 (TGF- β , Solarbio) with a final concentration of 10 ng/ml.

D. Three-dimensional microtissue formation and cell co-culture

Tumor microtissue was cultured in well-mesh microchip as follows: 200 μ L 2×10^5 /mL HCC827 and NCI-H460 cell suspension were added to the microwell array modified by 2% Pluronic F-127 (Sigma) solution, and after multiple days of culture, tumor microtissues were obtained. In cell co-culture study, the microtissues of HCC827 or NCI-H460 were obtained after 3 days of cell culture. Then 80 μ L Matrigel (B&D, Product code: 356237) was added in well-mesh microchip under ice bath conditions and then incubated at 37 °C for 20 min. Then 250 μ L of 2×10^5 /mL HUVEC cell suspension was added to the gelatinized Matrigel, to achieve three-dimensional co-culture of tumor microtissues and vascular endothelial cells *in vitro*.

E. Cell phenotype and live tracing

Immunofluorescence staining was used to detect the EMT-related protein E-cadherin expression of HCC827 and NCI-H460, platelet endothelial cell adhesion molecule (CD31), and tight junction protein (ZO-1) expression of the HUVECs. E-cadherin is a hallmark of EMT and generally its downregulation represents the emergence of EMT. CD31 is normally found on endothelial cells and makes up a large portion of endothelial cell intercellular junctions. ZO-1 is a peripheral membrane protein and also a tight junction-associated protein. Both CD31 and ZO-1 are used to characterize the

tight adhesion of vascular endothelial cells, which can be used to describe endothelial integrity.

Cells or microtissues were carefully rinsed with PBS and fixed with 4% paraformaldehyde (Sigma) for 20 min. Then goat serum solution for blocking (Abcam) was added, and the mixture was kept closed at room temperature for 1 h. A 1:100 primary antibody dilution solution (mouse anti-human E-cadherin, rabbit anti-human CD31, mouse anti-human ZO-1, Abcam) was added, and the mixture was left overnight at 4 °C, rinsed with PBS, supplemented with secondary antibody working solution (goat anti-mouse or anti-rabbit IgG) marked by Alexa Fluor 488 or Alexa Fluor 568, incubated at room temperature for 1 h, and then incubated at room temperature for 10 min after adding DAPI (Sigma) working solution. After rinsing with PBS three times, photos were taken by an inverted fluorescence microscope or a confocal microscope.

To determine cell migration, the living cells were marked with a fluorescent tracing dye. HCC827 cells were marked with Cell Tracker Green CMFDA (Life Invitrogen) using the following method: after culture for 3 days, HCC827 microtissues were formed in a well-mesh microchip; then, 1 μ g/mL Cell Tracker Green CMFDA serum-free medium was added and incubated at 37 °C for 30 min; after that, the fresh culture medium was replaced. We also used Cell Tracker Red CMTPX (Life Invitrogen) to mark HUVECs. The marking method was as follows: before being seeded, cells were placed in a serum-free culture medium and incubated with 1 μ g/mL Cell Tracker Red CMTPX at 37 °C for 30 min and then centrifuged; the fresh culture medium was replaced, and then the cells were resuspended for counting. After marking, cell migration

photos were taken with a confocal laser scanning microscope (FV3000, Olympus) on 0, 1, and 3 days.

F. Total RNA isolate and RT-qPCR

We separated total RNA from the no drug group and TGF- β group of HCC827 with TRIzol® reagent according to the manufacturer's instructions (Invitrogen). We used a One Step SYBR® PrimeScript™ RT-PCR kit (TaKaRa) to perform cDNA synthesis and PCR reaction on total RNA and used Lightcycle 96 (Roche) for detection. Average CT values were normalized to GAPDH expression levels. Primers synthesized by Sangon Biotech (Shanghai) Co., Ltd. were as follows:

Snail: 5'-TAGCGAGTGGTTCTGCG-3' (forward), 5'-AG GGCTGCTGGAAGGTAAAC-3' (reverse); GAPDH: 5'-CAATGAC CCCTTCATTGACC-3' (forward), 5'-GACAAGCTTCCGTT TCAG-3' (reverse); Akt: 5'-AGCCTGGGTCAAAGAAGTCA-3' (forward), 5'-TGTACTCCCCTCGTTGTGC-3' (reverse).

III. RESULTS AND DISCUSSION

A. Characterization of the well-mesh microchip

We developed a well-mesh microchip composed of four parts: a confocal dish with a central hole coated by PDMS, a PDMS microwell array membrane, a nylon mesh, and a PDMS cell culture medium storage layer, as shown in Fig. 1. Considering the working distance between the microscope and cells, we selected a confocal dish with a central hole as the carrier of the well-mesh microchip because a bottom layer that is too thick can influence cell imaging. The glass central hole of the confocal dish was coated with PDMS because a PDMS surface modified by Pluronic F-127 is superior to glass when cells are cultured to form spheroids or microtissues. In addition, because the confocal dish was used

as a carrier, the microwells in the PDMS microwell array membrane were hollow and could be penetrated, and microwell depth was dependent on the height of the prepared SU-8 template; measured by a step profiler, the depth was about 260 μm . The nylon mesh thickness was about 40 μm , and the pores were square, with a side length of 100 μm . The mesh was semipermeable to facilitate penetration by cell suspensions and culture mediums, and thus the cells could be cultured in microwells. When the microtissue reached a diameter greater than ~100 μm (over the mesh size), the mesh could keep the microtissues staying in the microwells. Overall, the main advantages of the establish chip are (1) the well-mesh microchip can directly form tumor microtissue and realize three-dimensional cell culture without scaffold materials *in vitro*; and (2) this cage-like structure facilitated the positioning of microtissues without damaging them, and the well-mesh microchip could realize *in situ* culture and observation and simplify subsequent operations.

B. Microtissue formation in well-mesh microchip

There are many methods of forming cell spheroids or microtissues in microwells using Pluronic F-127 or similar polymers to modify the PDMS surface, which makes it impossible for the cells to adhere to the PDMS surface and causes them to form spheroids or microtissues. In this study, we adopted a similar method and inoculated HCC827 and NCI-H460 cells in a well-mesh microchip. The HCC827 and NCI-H460 cell suspension was able to smoothly penetrate the nylon mesh pores (~100 μm) to enter the microwell modified by Pluronic F-127. After being cultured for 3 days, HCC827 and NCI-H460 cells formed microtissues. As the microtissues were far bigger than the size of the mesh pores, they were

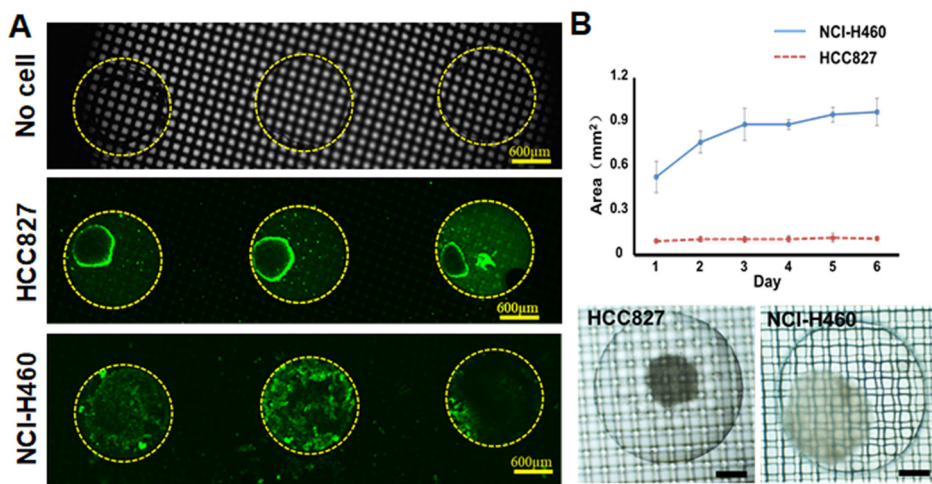


FIG. 2. (a) Fluorescence images of HCC827 and NCI-H460 microtissues stained by Cell Tracker Green CMFDA in a well-mesh microchip after 3 days culture; bar = 600 μm . (b) Area of HCC827 and NCI-H460 microtissues formed on different days, $n = 4$. Microtissues of HCC827 and NCI-H460 cells formed in a well-mesh microchip on day 6; bar = 300 μm .

trapped in the cage-like structure formed by the microwell and mesh. The results after 3 days of continuous culture are shown in Fig. 2(a). We stained microtissues by Cell Tracker Green CMFDA, and found bright fluorescence, showing that the cells had good viability.

In addition, we found that the two kinds of non-small-cell lung carcinoma cells had formed microtissues with greatly different appearances. By analyzing the area of the microtissues in microwell, as shown in Fig. 2(b) and in the [supplementary material](#), we found that the microtissues formed by HCC827 were smaller (less than 0.1 mm^2 , with diameters of $\sim 300\text{ }\mu\text{m}$), and there was no apparent change in size over multiple days' culture. From day 1 to day 6, the areas were from $0.096 \pm 0.007\text{ mm}^2$ to $0.111 \pm 0.010\text{ mm}^2$. In contrast, the size of the NCI-H460 cells reached 1 mm^2 , close to the microwell size; in the first 1 to 3 days of culture, the size increased significantly, and then after 3 days, their size remained relatively stable, entering a plateau period. On day 1, day 3, and day 6, the cell area is $0.529 \pm 0.106\text{ mm}^2$, $0.886 \pm 0.109\text{ mm}^2$, and $0.970 \pm 0.092\text{ mm}^2$, respectively.

C. Three-dimensional cell co-culture in well-mesh microchip

Following the tumor cell microtissue formation experiment, we studied the three-dimensional co-culture of lung tumor cell microtissues and vascular endothelial cells in a well-mesh microchip. We first added HCC827 cells or NCI-H460 cells into the modified well-mesh microchip. After 3 days of culture, tumor microtissues were obtained. The

microtissues were then stained with Cell Tracker Green CMFDA. Next, an appropriate amount of Matrigel was added under ice bath conditions and then incubated at 37°C for 20 min. The Matrigel changed from liquid to gel that encapsulated the microtissues and was able to reach the mesh position or slightly lower. Next, HUVECs marked with Cell Tracker Red CMTPX were inoculated into the gelatinous Matrigel to co-culture with HCC827 microtissues or NCI-H460 cell microtissues. The process is shown in Fig. 3(a). We used a confocal microscope to photograph the resulting three-dimensional cell co-culture model, as shown in Fig. 3(b). It can be clearly seen that HCC827 microtissues or NCI-H460 cell microtissues (green) have a distinct boundary layer with the HUVECs (red), which was formed by the gelatinous Matrigel and mesh. The HUVECs intercepted and located at the upper side of the Matrigel and mesh, and could not drop into the microwell. The HUVECs also formed a lattice due to the presence of the mesh, and partial HUVECs were present on the nylon mesh frame.

D. TGF- β -mediated cell EMT in well-mesh microchip

Epithelial-mesenchymal transition (EMT) was first noted in studies of cell migration during development. Some reports indicate that EMT during development is similar to tumor invasion, suggesting that tumor cell invasion or migration is a pathological EMT process, and epithelial-derived tumor cells can weaken the intercellular junction to obtain motor ability through EMT.²⁸ In this study, we investigated TGF- β -mediated lung tumor EMT through cell E-cadherin expression,

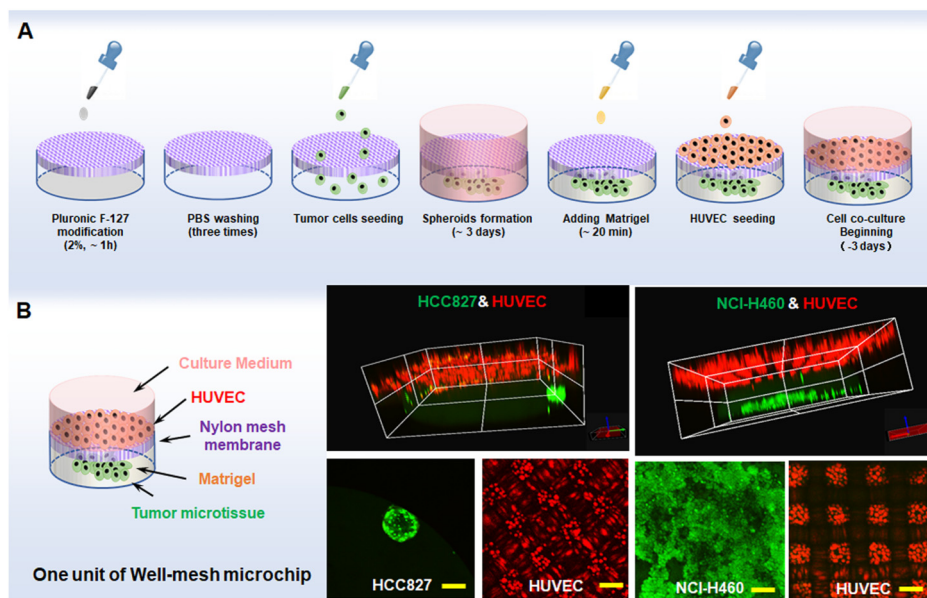


FIG. 3. (a) Tumor microtissue formation and three-dimensional co-culture process. (b) 3D/2D image of HCC827/NCI-H460 microtissues and HUVECs co-cultured in a well-mesh microchip. HCC827 cells or NCI-H460 stained with Cell Tracker Green CMFDA are green; HUVECs stained with Cell Tracker Red CMTPX are red; bar = $100\text{ }\mu\text{m}$.

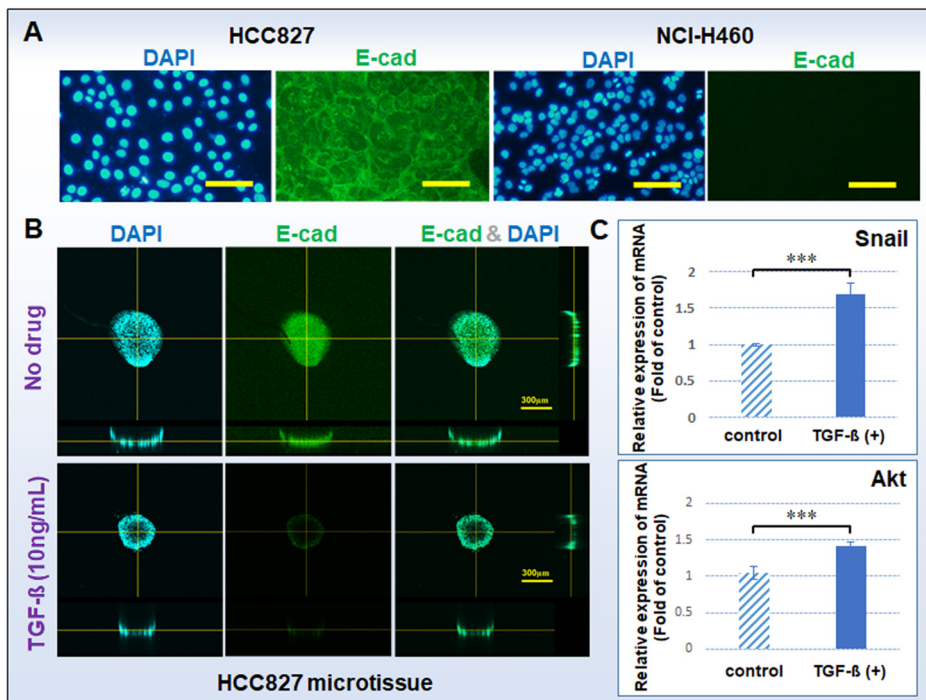


FIG. 4. (a) E-cadherin expressions of HCC827 and NCI-H460 cells cultured in a 2D plate; bar = 100 μ m. (b) E-cadherin expressions of microtissues of HCC827 with or without TGF- β cultured in a well-mesh microchip; bar = 300 μ m. E-cadherin: green; cell nucleus DAPI: blue. (c) Gene expression of Snail and Akt of HCC827 microtissues with or without TGF- β cultured in a well-mesh microchip. The standard errors were obtained from Student's t-test. n = 3; ***P < 0.005; GAPDH refers to the internal parameter; microtissue without TGF- β refers to the control group.

EMT-related gene expression, and tumor cell migration ability. First of all, the EMT-related protein E-cadherin was selected for immunofluorescence staining analysis, as shown in Fig. 4(a). E-cadherin is an epithelial marker protein and also an intercellular adhesive protein. Generally, a decrease or loss of E-cadherin as a hallmark event can further decrease adhesion between cells and promote tumor cell invasion and metastasis.²⁹ The positive E-cadherin expression cells is associated with cells that adhered more tightly. In this study, HCC827 cells were positive for E-cadherin expression, while NCI-H460 cells did not express E-cadherin. NCI-H460 cells that did not express E-cadherin were not suitable for this study, so we only use HCC827 cells to complete the follow-up experiments. In addition, we suspect that the difference in protein expression of E-cad also causes differences in the morphology of the HCC827 and NCI-H460 microtissues.

To demonstrate the cell EMT in the established well-mesh microchip, we added TGF- β as an experimental drug treatment. TGF- β is a growth factor widely used to regulate cell growth and differentiation and it promotes the development of EMT. A large number of studies have reported that the application of TGF- β will result in the loss of E-cadherin expression in epithelial cells or epithelial-derived tumor cells, to further lead to EMT. The results, shown in Fig. 4(b), indicate that with TGF- β treatment, the E-cadherin expression of

HCC827 microtissue in well-mesh microchip decreased. In addition, during tumor formation and development, tumor cells undergo EMT and mesenchymal-epithelial transition (MET) processes repeatedly, and these processes include abnormal activation of multiple transcription factors, such as Snail (Snail-1) and Akt, changes in cell surface protein expression, and reorganization of cytoskeletal proteins, which are important processes for tumor invasion, spread, and metastasis and closely associated with tumor cells themselves. We used real-time qPCR to detect Snail and Akt gene expression in HCC827 microtissue with and without TGF- β , as shown in Fig. 4(c). The transcription factor Snail and Akt have inverse relationships with E-cadherin at the mRNA and protein levels in most epithelial cancer cells. Studies have shown that the expression of Snail and Akt is at the core of lung cancer EMT and metastasis.³⁰ The results showed that TGF- β can promote Snail and Akt expression to inhibit E-cadherin expression, resulting in cell EMT.

In addition, we also used the established well-mesh microchip to perform the cell migration experiment, as shown in Fig. 5(a). We performed a slice scan using a confocal microscope with a scan accuracy of 5 μ m/slides. The HUVEC position was determined to be 0 μ m, and the site of tumor microtissue near to the HUVEC was determined to be "x" μ m. We observed the cell migration by "x" change on days 0, 1,

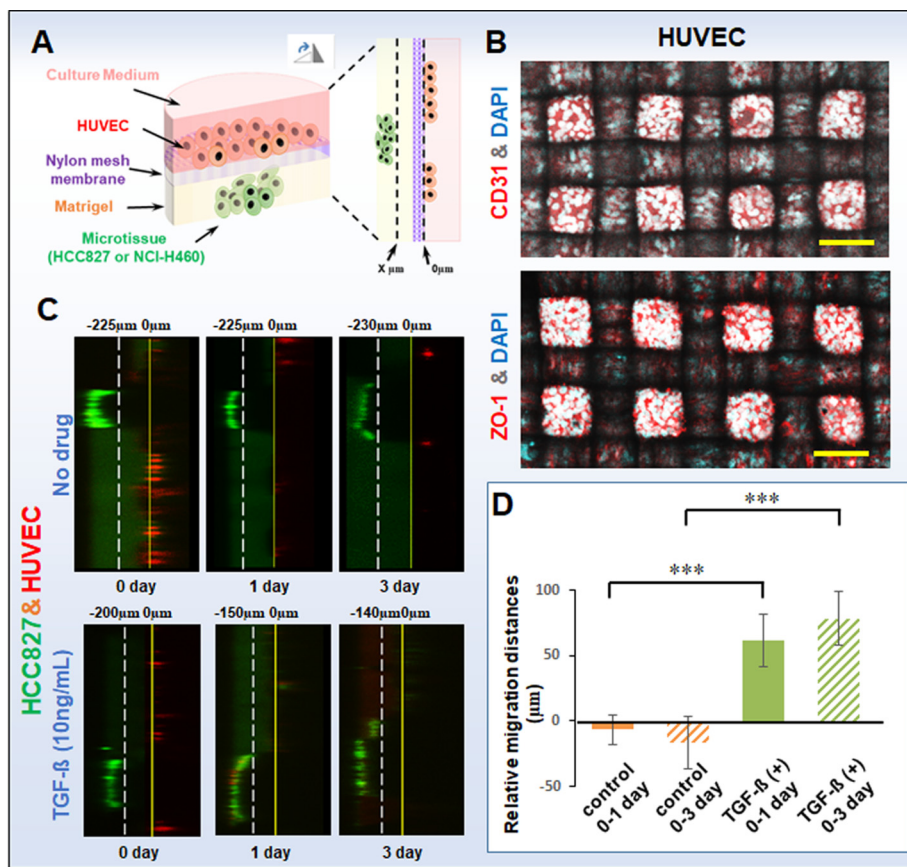


FIG. 5. (a) Schematic of migration of tumor cell microtissues under cell co-culture in a well-mesh microchip. The HUVEC position was determined to be $0\text{ }\mu\text{m}$, and the site of tumor microtissue near to the HUVEC was determined to be “x” μm . We observed the cell migration by “x” change on days 0, 1, and 3. (b) CD31 and ZO-1 expression of HUVECs. CD31 or ZO-1: red; cell nucleus DAPI: blue. (c) Migration images of HCC827 microtissue with or without TGF- β . HCC827: green; HUVEC: red; bar = $100\text{ }\mu\text{m}$. A slice scan was performed by using a confocal microscope with a scan accuracy of $5\text{ }\mu\text{m}/\text{slide}$. (d) Histogram of migration distances of HCC827 microtissue with or without TGF- β . The standard errors were obtained from Student’s t-test. n = 3; ***P < 0.005; Microtissue without TGF- β refers to the control group.

and 3. Furthermore, we found that the tumor microtissue was thick and opaque, which impeded observation of the relative position of the HUVECs. In addition, as the cell migration was shown in the longitudinal section, only a small amount of the HUVECs could be observed. To determine the integrity of the endothelial layer, we characterized the platelet-endothelial cell adhesion molecule-1 (PECAM-1 or CD31) and the tight junction protein ZO-1 in HUVECs, as shown in Fig. 5(b), in which it can be seen that the HUVEC cells are closely arranged and the endothelial layer is intact. The cell migration results are shown in Figs. 5(c) and 5(d). In the groups without TGF- β , the HCC827 cells hardly moved from day 0 to day 1 or day 3 ($-6.7 \pm 11.5\text{ }\mu\text{m}$ and $-16.7 \pm 20.2\text{ }\mu\text{m}$, respectively), while with TGF- β treatment, the migration ability was greatly enhanced, with apparent migration from day 0 to day 1 and from day 0 to day 3 ($61.7 \pm 20.2\text{ }\mu\text{m}$ and $78.3 \pm 20.2\text{ }\mu\text{m}$, respectively). The histogram data of migration distances of HCC827 microtissue with or without TGF- β also shows similar results,

indicating that the migration capacity of microtissues increased significantly with TGF- β treatment. Furthermore, this result is consistent with the expression of E-cadherin of HCC827 microtissue with or without TGF- β .

IV. CONCLUSION

In this study, we developed a well-mesh three-dimensional cell culture microchip to realize microtissue formation *in vitro*. Two kinds of non-small-cell lung cancer cell line (adenocarcinoma HCC827 cells and large-cell lung cancer NCI-H460 cells) were used to form tumor microtissues in the experiments. In addition, in the established microchip, we achieved the creation of a biomimetic three-dimensional multi-factor tumor microenvironment, including tumor cell microtissues, an extracellular matrix, vascular endothelial cells, and growth factor. The tumor cell migration and gene expression were investigated, and it was verified that TGF- β

induced HCC827 cells to activate the Snail and Akt gene, promoting EMT with the decrease of E-cadherin expression. This model can be used for the formation of three-dimensional microtissues *in vitro* and the construction of biomimetic micro-environments, and thus has potential application value in areas such as *in vitro* organ chips, tissue engineering, and drug evaluation.

SUPPLEMENTARY MATERIAL

See [supplementary material](#) for images of microtissues formation of HCC827 and NCI-H460 in a modified microwell at different days.

ACKNOWLEDGMENTS

This research was supported by the National Natural Science Foundation of China (NNSFC) (Grant No. 31800848), Shanghai Municipal Science and Technology Commission (No. 16DZ2260601), Natural Science Foundation of Shanghai (No. 15JC1400303), and Materials Genome Institute, Shanghai University.

REFERENCES

- ¹M. Marimuthu and S. Kim, *Anal. Biochem.* **413**(2), 81–89 (2011).
- ²T. Kim, I. Doh, and Y. H. Cho, *Biomicrofluidics* **6**(3), 34107 (2012).
- ³Y. S. Sun, S. W. Peng, K. H. Lin, and J. Y. Cheng, *Biomicrofluidics* **6**(1), 014102 (2012).
- ⁴W. Asghar, R. El Assal, H. Shafiee, S. Pitteri, R. Paulmurugan, and U. Demirci, *Mater. Today* **18**(10), 539–553 (2015).
- ⁵X. J. Li, A. V. Valadez, P. Zuo, and Z. Nie, *Bioanalysis* **4**(12), 1509–1525 (2012).
- ⁶D. Huh, G. A. Hamilton, and D. E. Ingber, *Trends Cell Biol.* **21**(12), 745–754 (2011).
- ⁷H.-S. Hou, H.-F. Tsai, H.-T. Chiu, and J.-Y. Cheng, *Biomicrofluidics* **8**(5), 052007 (2014).
- ⁸N. Peela, D. Truong, H. Saini, H. Chu, S. Mashaghi, S. L. Ham, S. Singh, H. Tavana, B. Mosadegh, and M. Nikkhah, *Biomaterials* **133**, 176–207 (2017).
- ⁹X. Yang, K. Li, X. Zhang, C. Liu, B. Guo, W. Wen, and X. Gao, *Lab Chip* **18**(3), 486–495 (2018).
- ¹⁰M. Cavo, M. Caria, I. Pulsoni, F. Beltrame, M. Fato, and S. Scaglione, *Sci. Rep.* **8**(1), 5333 (2018).
- ¹¹S. Oh, H. Ryu, D. Tahk, J. Ko, Y. Chung, H. K. Lee, T. R. Lee, and N. L. Jeon, *Lab Chip* **17**(20), 3405–3414 (2017).
- ¹²Y. Wang, X. Yuan, K. Yu, H. Meng, Y. Zheng, J. Peng, S. Lu, X. Liu, Y. Xie, and K. Qiao, *Biomaterials* **171**, 118–132 (2018).
- ¹³S. M. Ong, C. Zhang, Y. C. Toh, S. H. Kim, H. L. Foo, C. H. Tan, D. van Noort, S. Park, and H. Yu, *Biomaterials* **29**(22), 3237–3244 (2008).
- ¹⁴D. Huh, Y. S. Torisawa, G. A. Hamilton, H. J. Kim, and D. E. Ingber, *Lab Chip* **12**(12), 2156–2164 (2012).
- ¹⁵H. M. M. Ahmed, S. Salerno, A. Piscioneri, S. Khakpour, L. Giorno, and L. De Bartolo, *Colloids Surf. B Biointerfaces* **160**, 272–280 (2017).
- ¹⁶D. T. T. Phan, X. Wang, B. M. Craver, A. Sobrino, D. Zhao, J. C. Chen, L. Y. N. Lee, S. C. George, A. P. Lee, and C. C. W. Hughes, *Lab Chip* **17**(3), 511–520 (2017).
- ¹⁷H. Zhang, L. Xiao, Q. Li, X. Qi, and A. Zhou, *Biomicrofluidics* **12**(2), 024119 (2018).
- ¹⁸F. Schulze, X. Gao, D. Virzonis, S. Damiani, M. R. Schneider, and R. Kodzius, *Genes* **8**(10), 244 (2017).
- ¹⁹A. Zuchowska, E. Jastrzebska, K. Zukowski, M. Chudy, A. Dybko, and Z. Brzozka, *Biomicrofluidics* **11**(2), 024110 (2017).
- ²⁰M. J. Bissell and D. Radisky, *Nat. Rev. Cancer* **1**(1), 46–54 (2001).
- ²¹H. F. Dvorak, V. M. Weaver, T. D. Tilley, and G. Bergers, *J. Surg. Oncol.* **103**(6), 468–474 (2011).
- ²²C. Lorenzo, C. Frongia, R. Jorand, J. Fehrenbach, P. Weiss, A. Maandhui, G. Gay, B. Ducommun, and V. Lobjois, *Cell Div.* **6**, 22 (2011).
- ²³Z. Xu, Y. Gao, Y. Hao, E. Li, Y. Wang, J. Zhang, W. Wang, Z. Gao, and Q. Wang, *Biomaterials* **34**(16), 4109–4117 (2013).
- ²⁴S. P. Carey, A. Starchenko, A. L. McGregor, and C. A. Reinhart-King, *Clin. Exp. Metastasis* **30**(5), 615–630 (2013).
- ²⁵A. Guzman, V. Sanchez Alemany, Y. Nguyen, C. R. Zhang, and L. J. Kaufman, *Biomaterials* **115**, 19–29 (2017).
- ²⁶X. Yang, X. Xu, Y. Zhang, W. Wen, and X. Gao, *Genes* **8**(9), 218 (2017).
- ²⁷X. Wan, Z. Li, H. Ye, and Z. Cui, *Biotechnol. Lett.* **38**(8), 1389–1395 (2016).
- ²⁸S. Gurzu, S. Turdean, A. Kovacs, A. O. Contac, and I. Jung, *World J Clin. Cases* **3**(5), 393–404 (2015).
- ²⁹R. Kalluri and R. A. Weinberg, *J. Clin. Investig.* **119**(6), 1420–1428 (2009).
- ³⁰S. Lamouille, J. Xu, and R. Deryck, *Nat. Rev. Mol. Cell Biol.* **15**(3), 178–196 (2014).